Orientation of aromatic residues in amyloid cores: Structural insights into prion fiber diversity

Orientation of aromatic residues in amyloid cores: Structural insights into prion fiber diversity

Anna Reymer[a,1,2], Kendra K. Frederick[b,c], Sandra Rocha[a], Tamás Beke-Somfai[a], Catherine C. Kitts[a], Susan Lindquist[b,c,d], and Bengt Nordén[a,1]

[a]Department of Chemical and Biological Engineering, Chalmers University of Technology, SE-41296 Gothenburg, Sweden; [b]Whitehead Institute for Biomedical Research, Cambridge, MA 02142; and [c]Howard Hughes Medical Institute and [d]Department of Biology, Massachusetts Institute of Technology, Cambridge, MA 02139

Edited by Alan R. Fersht, Medical Research Council Laboratory of Molecular Biology, Cambridge, United Kingdom, and approved October 22, 2014 (received for review August 20, 2014)

Structural conversion of one given protein sequence into different amyloid states, resulting in distinct phenotypes, is one of the most intriguing phenomena of protein biology. Despite great efforts the structural origin of prion diversity remains elusive, mainly because amyloids are insoluble yet noncrystalline and therefore not easily amenable to traditional structural-biology methods. We investigate two different phenotypic prion strains, weak and strong, of yeast translation termination factor Sup35 with respect to angular orientation of tyrosines using polarized light spectroscopy. By applying a combination of alignment methods the degree of fiber orientation can be assessed, which allows a relatively accurate determination of the aromatic ring angles. Surprisingly, the strains show identical average orientations of the tyrosines, which are evenly spread through the amyloid core. Small variations between the two strains are related to the local environment of a fraction of tyrosines outside the core, potentially reflecting differences in fibril packing.

linear dichroism | polarized light | prion proteins | Sup35 strains | tyrosine

Amyloids comprise a diverse group of protein polymers characterized by beta-strands that run perpendicular to the polymeric fiber axis. They are associated with devastating economic hardship in an extraordinary variety of settings—ranging from the degenerative diseases of our aging population (1) to the bacterial biofilms that resist eradication by antibiotics, bacteriophage, and even bleach (2). However, amyloids also provide beneficial functions; for example, they help to maintain long-term neuronal synapses (3, 4). Amyloid proteins are the structural basis for a paradigm shift in microbial genetics: Conformational changes of self-templating amyloids form protein-based elements of inheritance, known as "prions" (5–7), that create phenotypic diversity in changing environments (8, 9). A peculiar, and still mysterious, property of prions (and virtually all amyloidogenic proteins) is the ability of the same polypeptide chain to stably adopt distinct amyloid folds with different physical and biological properties (10–12). These are referred to as prion "strains" and are named for the distinct biological phenotypes they confer. Amyloid strains were first described for the mammalian prion protein PrP, which is responsible for transmissible spongiform encephalopathy (13, 14). They now seem to be a general property of amyloids associated with various neurodegenerative diseases (15–18). Indeed, many of these have prion-like self-templating dispersion properties in vivo that are associated with different disease phenotypes (19–21).

However, despite the importance of amyloids in so many aspects of biology, the amyloid fold remains one of the most poorly understood of all basic protein folds. This is mainly because the methods for structural characterization of such insoluble polymers are limited. Here, by using a structural probe of amyloid fibers and two mechanisms of fiber orientation, we demonstrate the utility of polarized-light spectroscopy measurements (linear dichroism, LD) to determine accurate angular data of aromatic side groups in amyloid fibers. We apply this method to amyloid fibers of the yeast prion protein Sup35, the translation termination factor in yeast. Sup35 has three functional domains: an amyloid forming amino-terminal domain (N), a highly charged middle domain (M), and a carboxyl-terminal domain (C), which is involved in translation termination. Tyrosines are well distributed in the amyloid-forming domain of the protein, providing plentiful structural probes in the amyloid core (Fig. 1*A*). The N and M domains (Sup35NM) are responsible for the prion activity. When Sup35 switches from its native conformation to an amyloid form, the fidelity of translation termination changes and new phenotypes are created (9). Upon conversion into a prion state Sup35NM can adopt a variety of distinct amyloid-rich fiber conformations. There are at least two fiber forms of Sup35NM, called "weak" and "strong" for the phenotypes they confer in vivo rather than for their biophysical properties (10). For example, amyloids that confer a strong phenotype are biophysically more fragile. More Sup35 is therefore sequestered in the amyloid form owing to an increase in fiber ends, resulting in stronger stop-codon read-through phenotypes in vivo. The amino acids that control the conformational switch have been delineated but their structural constraints are only loosely defined (22–25). LD, defined as the differential absorption between light polarized, parallel and perpendicular to a macroscopic orientation direction, revealed a general structural feature of amyloids. Moreover, the

Significance

Amyloids, which are protein fiber aggregates, are often associated with neurodegenerative diseases such as Alzheimer's, but they can also be beneficial, as in yeasts, where they help cells adapt to environmental changes. Intriguingly, the same protein has the ability to aggregate into different fiber forms, known as strains, that generate distinct biological phenotypes. Structurally, little is known about strains. Using polarized light spectroscopy, we provide structural information on two distinct phenotypic strains of the yeast translation termination factor, Sup35. Remarkably, they show similar orientation of aromatic residues in the fiber core relative to the fiber direction, suggesting similar structures. Small variations are observed, indicating different local environments for aromatic residues outside the core, reflecting differences in fiber packing.

Author contributions: A.R., S.R., and B.N. designed research; A.R. and K.K.F. performed research; A.R., K.K.F., S.R., T.B.-S., C.C.K., S.L., and B.N. analyzed data; and A.R., K.K.F., S.R., T.B.-S., S.L., and B.N. wrote the paper.

The authors declare no conflict of interest.

This article is a PNAS Direct Submission.

[1]To whom correspondence may be addressed. Email: reymer@chalmers.se or norden@chalmers.se.

[2]Present address: Bases Moléculaires et Structurales des Systèmes Infectieux, Université Lyon 1/CNRS UMR 5086, IBCP,7 Passage du Vercors, Lyon 69367, France.

This article contains supporting information online at www.pnas.org/lookup/suppl/doi:10.1073/pnas.1415663111/-/DCSupplemental.

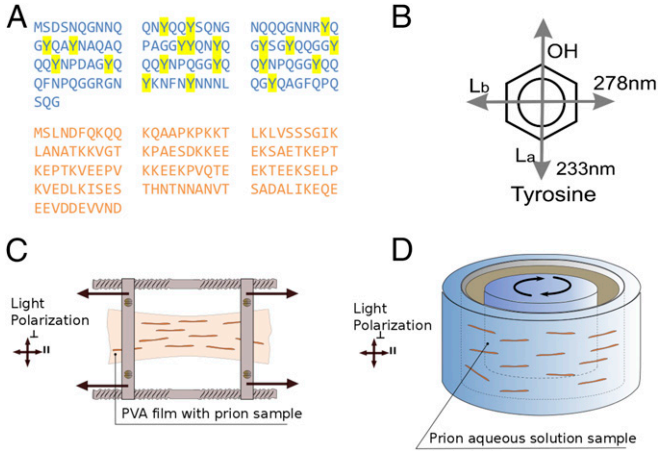

Fig. 1. Principles of polarized light measurements. (*A*) Sequence of NM domain (residues 1–253) of yeast Sup35 prion protein. N domain is shown in blue with tyrosine (Y) residues (whose orientation is detected by LD) highlighted with yellow. (*B*) Transition dipole moments of UV transitions L_a and L_b of tyrosine chromophore. (*C* and *D*) The two alignment techniques used in the study: orientation in a stretched film (*C*) and in a Couette shear flow cell (*D*).

method is sensitive enough to characterize structural variations between strains.

Results

Principles for Determining the Orientation of Chromophores in Fibers. LD reports on the orientation of the electronic transition moments of molecular chromophores in a macroscopically oriented sample. For prion fibers the orientation was attained with a Couette shear flow cell and a stretched polymer matrix. To characterize the tyrosine orientation we use nonempirical assignment of fiber order parameters in flow-oriented solution in the presence of sucrose, and in stretched poly(vinyl alcohol) (PVA) hydrogel environments (Fig. 1). In a hydrodynamic flow field the orientation of a fiber is described in terms of two angular coordinates with respect to the coordinate system of the flow cell: angles between the fiber orientation axis and the Couette cylinder axis or the flow orientation. In a polymeric matrix the distribution symmetry of oriented fibers is uniaxial and therefore depends only on a single angular coordinate: angle between the fiber and the macroscopic orientation direction. Previous LD studies on amyloid samples, oriented by shear flow, are merely qualitative because the degree of alignment of the fibers could not be quantified (26–28). Without this orientation parameter it is not possible to deduce how the transition moments of chromophores are oriented in the fiber coordinate framework (Eq. **1** and *Supporting Information*). Additional limitations are poor fiber orientation attained by shear flow and significant increase in background scattering by the fibers, resulting in spectra of poor quality (26–28). By using a structural probe (thioflavin T, ThT) and exploiting the two different mechanisms for fiber orientation—shear-flow in the presence of sucrose and stretched polymer matrix—we attain tyrosine orientation distribution in prion fibers, which represents, to our knowledge, the first detailed, experimentally quantitative information determined by LD of the local organization of amyloids.

The orientation of a tyrosine chromophore in a protein aggregate is described by two angular coordinates: the angles that the transition moments of the UV absorption bands L_a (absorbing at 233 nm) and L_b (278 nm) make with respect to the prion fiber axis. The transition moments are directed orthogonal to each other in the plane of the benzene ring of tyrosine (Fig. 1*B*). Because there is no spectral overlap with other transitions at these wavelengths the angular coordinates may be determined from the relation

$$LD(\lambda_i)/A_{iso}(\lambda_i) = 1.5\, S\left(3\langle\cos^2\phi(\lambda_i)\rangle - 1\right). \quad [1]$$

Here LD is the differential absorbance of orthogonal forms of polarized light at wavelength λ_i, A_{iso} is the absorbance of the isotropic sample, $\phi(\lambda_i)$ is the angle between the fiber axis and the direction of the transition moment, and S is an order parameter defining the degree of orientation of fibers in the sample. In the case of a prion fiber we regard S as the product of two order parameters, allowing some disorder owing to the arrangement of regularly structured protein monomers inside the fibrous aggregate (for details, see *Supporting Information*):

$$S = S_g S_i, \quad [2]$$

where S_g is the macroscopic (global) order parameter of fibrous aggregates and S_i is an internal order parameter characterizing the orientation of local monomeric aggregates within a fiber. S_i is thus a "microscopic" orientation factor relating the orientation of the monomers to a local fiber axis direction, p, and the factor S_g relates p to the stretching direction (the long axis of the fiber). In the limit of high shear rates in solution, or infinite stretch of the polymer matrix, $S_g = 1$ corresponds to a perfect orientation of the fibrous particles parallel with the flow direction or the stretch direction in the two systems, respectively. S_g can be seen as a measure of hydrodynamic properties of the fibrous assemblies in solution or their straightness in the gel matrix. S_i takes also values between the limits 0 and 1 corresponding, respectively, to isotropic and to perfect orientation of the unique axis of the monomer parallel to the local polymer axis.

The tyrosine orientation angles are obtained by determining the parameter S and then solving Eq. **1** for the angle $\phi(\lambda_i)$. S_g is directly related to the second moment (P_2) of the orientation distribution function of the fibers, which we here determine using two independent approaches. In the flow experiments, S_g is calculated using an orientation distribution model for rigid ellipsoidal particles in laminar flow (see *Supporting Information* for details). In the PVA gel, S_g is determined by a distribution model for uniaxial stretch deformation (29, 30). There is a significant difference between the two alignment methods: The stretch angular distribution does not depend on the length of the particles, whereas the hydrodynamic model does, and the longer the particles the better their flow orientation. For the prion fibers there is naturally a length distribution, which will affect S_g in solution but not in a PVA gel. There is also a characteristic morphology, affecting S_i, which potentially depends on the fiber assembly mechanisms and fibrillization history. Similar S_i values suggest similar morphological behaviors. However, different S_i values will reflect morphological differences with respect to fiber organization. Independent evidence from the nonempirical determination of orientation parameter S_g in PVA as well as from the sucrose flow experiment (*Supporting Information*) allows S_i to be determined.

Fiber Order Parameters and Angular Orientation of Tyrosines. The S factor of the fibers was first obtained in aqueous solution in the presence of ThT from the LD and absorbance spectra (Fig. 2). Upon binding to amyloid fibers the transition moment of ThT is oriented nearly parallel to the fiber axis, $\phi(\lambda_i) = 0$–$20°$, and thus the LD/A_{iso} at 440 nm can be used to determine S from Eq. **1** (31).

Knowing the S factor, calculated by using ThT, the angle $\phi(\lambda_i)$ for tyrosine L_b was obtained from the LD/A_{iso} amplitude at 278 nm (Fig. 2) and was about 30° for both strains (Table 1). Because the L_b transition lies in the plane of a phenyl ring of tyrosine (Fig. 1) and might thus be subject to more or less free rotation, the L_a transition is also required to uniquely identify the orientation of a tyrosine moiety in a 3D structure. Owing to strong light scattering at shorter wavelength and overlapping absorption

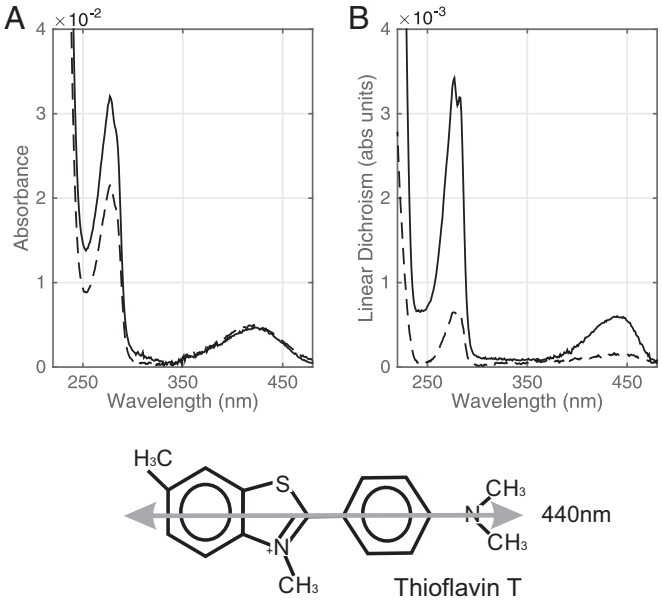

Fig. 2. Binding of ThT to prion fibers. Absorbance (*A*) and LD (*B*) spectra of weak (solid line) and strong (dashed line) Sup35NM fibers in aqueous solution in presence of ThT under an applied shear force of 3,100 s^{-1}. The transition dipole moments of the electronic transitions of ThT are depicted at the bottom.

in the presence of ThT, the L_a band is completely obscured under these conditions. Hence, spectra of fibers were recorded, without ThT bound, in aqueous sucrose solution under shear flow and in a stretched PVA matrix. Sucrose works as a refractive index matching medium reducing the light scattering from fibers and increases the flow orientation of the fibers. The use of refractive index matching solvents in LD has been previously suggested for samples of phosphatidylcholine vesicles to detect LD bands in the peptide-absorbing region (200–230 nm) (32). Sucrose reduced the scattering induced by liposomes without significantly altering their properties and increased the LD signal owing to increased viscous shear forces. Measurements using PVA and sucrose solution provide independent modes of determining the orientation parameter S_g. S_i values are then obtained from Eq. **1** by inserting S_g (as a component of S) and the tyrosine L_b angle value, experimentally determined using ThT probe.

The spectra of the two fiber forms were similar for both orientation techniques and showed the characteristic positive LD in the L_b band region 250–290 nm, a negative LD in the L_a region 220–250 nm, and identical L_a/L_b intensity ratio (Fig. 3). Accordingly, the angle L_a of the long axis of tyrosine, which coincides with Cβ–Cγ bond, was also similar for both strains and was 60° (Table 1). The S factor is higher in the presence of sucrose and PVA than in aqueous solution owing to a better alignment of the fibers in those conditions. S_g values obtained from the flow experiments reflect the length variation of the fibers. S_g of weak strain resulted in estimated lengths twice as long as the strong fibers, a conclusion that is in harmony with their different physical properties and defines their different activities in vivo (33, 34). There is no significant difference between the S_i values of strong and weak fiber forms, which is an indication of similar arrangement of structured protein monomers in the two strains.

LD reports on angular orientation only of oriented residues; other randomly oriented chromophores will have zero LD signal. Our data indicate that the fraction of well-oriented tyrosine residues is in similar structural environments in both strains. The small value of the L_b angle of tyrosine residues in prion fibers suggests a rather narrow angular coordinate distribution. If there had been free rotation around the C_β–C_γ bond, an L_b angle close to 50° would have been obtained, given the 60° of the L_a transition moment angle. The narrow angle distribution is consistent with the stacking arrangements of the aromatic side chains.

Local Environments of Tyrosine Residues. Whereas the global character of the spectra suggested a general structural motif for the organization of aromatic rings in amyloid fibers, LD was sensitive enough to report on structural variations owing to different underlying environments between fiber forms. We observed for the L_b transition a difference between the LD and absorption bands, resulting in a wavelength dependence of the ratio LD/A_{iso}, more pronounced in the weak prion. The L_b LD band exhibits a more pronounced vibrational structure than the absorption band. This result indicates that the orientation distribution of tyrosine L_b transition moment is also accompanied by some environmental distribution. Whereas the absorption band is broader owing to inhomogeneous broadening—different tyrosine chromophores experiencing somewhat different environments—the LD band reflects a systematic correlation between environment and orientation. The variation of LD/A_{iso} ratio with the wavelength may be accounted for by an inhomogeneous solvent effect in terms of curve modeling (Fig. 4). The analysis is based on a spectrum of *p*-methylphenol in hexane, taken as a model of tyrosine in a nonpolar environment (note the pronounced vibrational fine structure of the L_b band, Fig. 4*B*). This well-resolved spectrum can be made similar to the absorption and LD spectra that we observe for the prion samples by simply overlaying a set of copies with infinitesimally different wavelength shifts (i.e., simulating many slightly different local environments that tyrosine side chains might experience). As opposed to the absorption bands, the LD bands of the strains have different profiles, which indeed supports the fact that some tyrosine residues are experiencing different environments. This is consistent with recent studies that establish that many side chains in the two fiber forms are exposed to different chemical environments (25). From amide hydrogen/deuterium exchange

Table 1. Angles of tyrosine transition dipole moments, L_a and L_b, relative to the fiber axis, and order parameters S, S_g, and S_i of weak and strong Sup35 prion strains

Alignment technique	Phenotype	L_a (232 nm), °	L_b (278 nm), °	S	S_g	S_i
Aqueous solution with ThT	Weak	N/A	31–36	0.06	N/A	N/A
	Strong	N/A	27–33	0.017	N/A	N/A
Sucrose solution	Weak	58–59	31–36	0.13	0.60	0.22
	Strong	59–61	27–33	0.09	0.42	0.20
PVA humid gel	Weak	60–61	31–36	0.14	0.63	0.22
	Strong	61–62	27–33	0.12	0.62	0.19

As determined in solution in the presence of ThT or in sucrose solution and in stretched humid PVA matrix. Angle ranges refer to error estimates of LD^r and S (see Fig. S1 for details). N/A, not assessed.

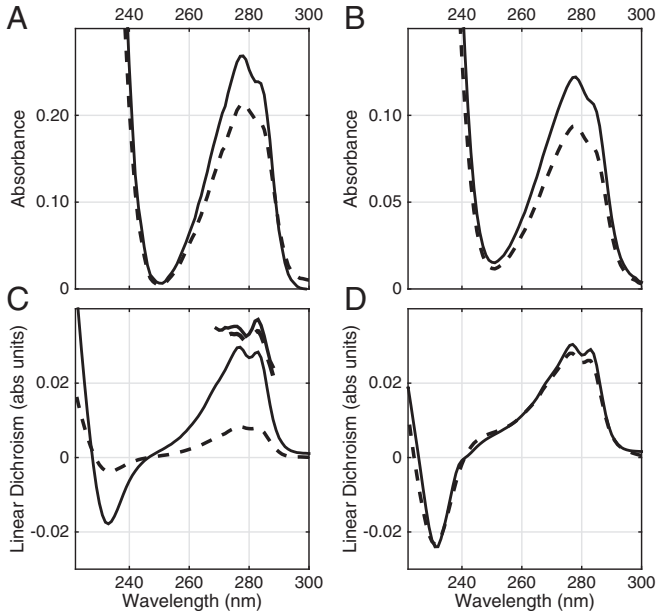

Fig. 3. Prion strains exhibit identical average tyrosine orientation. Absorbance (*A* and *B*) and LD (*C* and *D*) spectra of weak (solid line) and strong (dashed line) Sup35NM fibers in aqueous sucrose solution (*Left*) and in stretched humid film of PVA (*Right*). LD/A_{iso} ratio for both strains in flow-oriented solution is plotted over the L_b absorption band at 280 nm in *C*.

studies we know that the two strains share a tightly packed amyloid-rich core that is highly protected from the outside environment: for the strong strain, residues 1–40, and for the weak strain, residues 1–70 (23). A recent study using magic angle spinning NMR nuances this view. The N domain is dynamically rich, with regions that are ordered on the microsecond or longer timescales as well as regions ordered on somewhat shorter "intermediate" timescales (25). Tyrosine residues participate in both regions, although the weak strain has more sites that are ordered on longer timescales than the strong. Accordingly, some tyrosines show different chemical environments in the two strains (also demonstrated by small differences between the LD and absorbance spectra), suggesting that they may have distinct sheet–sheet interfaces (23, 25).

Discussion

We have outlined a generally applicable method to gain further structural insight into the structure of amyloid fibers. Amyloid fibers are defined by their beta-sheet content. We add that a general feature of this fold is the stacking of aromatic rings with a relatively defined geometry. This work suggests that in addition to a cross-beta arrangement of the protein backbone aromatic rings are arranged at a 60°/30° orientation relative to the fiber axis (Fig. 5). Moreover, this sensitive spectroscopic technique further permits detection of local environmental variations of amino acid side groups that are likely at the core of the prion strain phenomena.

Determining the spatial arrangement of aromatic residues in amyloid fibers will help to build models of fiber structure. It has been proposed that aromatic residues may have an important role in fiber assembly (35, 36). The attractive nonbonded interactions—π-stacking interactions—between the aromatic rings are suggested to contribute to stacking energy and order of amyloid fibers (35). The most common π-stacking geometry in proteins is the off-centered parallel orientation (parallel displaced) (37). Distance constraints attained by solid-state NMR spectroscopy for the phenylalanine residue of a short sequence of amylin (islet amyloid polypeptide) suggested that the beta-sheets are stacked side-by-side and the aromatic rings are facing the hydrophobic core of the fiber with distances between the rings of adjacent sheets of <6.5 Å (36). Our L_b angles for tyrosine residues in Sup35NM fibers are consistent with stacking interactions that preferentially orient the tyrosine planes parallel with the fiber axis, as proposed in those previous studies (Fig. 5). LD data point to a common structural arrangement of the aromatic side chains in the weak and strong strains of Sup35 prions, which might be extended to other amyloid-prone sequences because the LD spectra of glucagon (27), β_2-microglobulin (26), and a short sequence of the amyloid-β peptide (28) closely resemble those observed here for the Sup35 strains.

Differences between amyloid-based prion strains are thought to be a result of differences in packing interactions in the fiber. Our analysis of the LD/A_{iso} ratio shows that some tyrosines in the prion fiber forms experience environmental variations. According to quantum chemical calculations for *p*-methylphenol, a chromophore of tyrosine, a symmetric broadening of UV bands is expected in a hydroxyl polar environment: Hydrogen bonding between the phenol OH hydrogen and an external oxygen atom is predicted to give a red shift, whereas hydrogen bonding between phenol oxygen and a hydrogen of an OH group is expected to give a blue shift of similar magnitude (2–4 nm) (38). If all tyrosines had been oriented at the same angle and exposed to similar local environments, then the LD spectrum would have had the same shape as the (smeared) absorption spectrum, and LD/A_{iso} had been constant. However, if differently shifted tyrosines are also somehow differently oriented, the characteristic wavelength dependence that is observed in the prion LD spectrum can be reproduced. Only a superposition of LD spectra with different amplitudes [different $\phi(\lambda_i)$ values] and with shapes corresponding to differently shifted absorptions can explain the

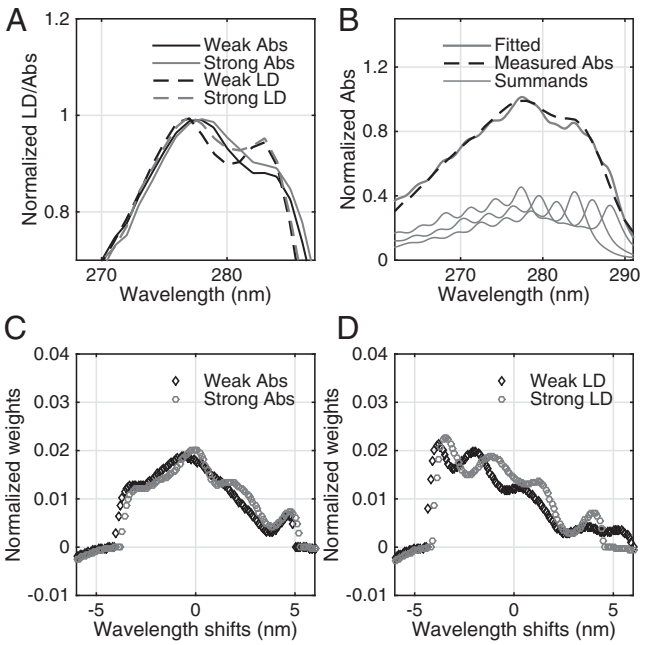

Fig. 4. Evidence for environmental inhomogeneity of tyrosine chromophores in the weak and strong strains of yeast Sup35NM fibers. (*A*) LD of L_b band is 1–2 nm narrower and blue-shifted in comparison with absorption spectra. The effect is more pronounced for the weak strain. (*B*) Principle of inhomogeneous broadening of tyrosine absorption modeled using *p*-methylphenol in hexane. (*C* and *D*) Spectral component analysis of absorbance (*C*) and LD (*D*) from subensembles of different shifts (environments) using the absorbance spectrum of *p*-methylphenol in hexane as a base vector.

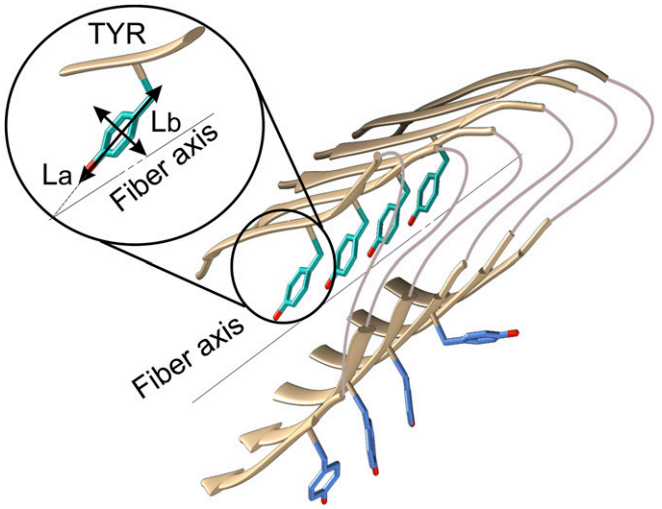

Fig. 5. Orientation of tyrosine residues in amyloid Sup35 prion strains. In the weak and strong fiber forms the tyrosine residues that are buried in the interior of the fiber have average L_b and L_a angular coordinates of 30°± 2° and 60°± 2°, respectively, suggesting identical or nearly identical local organizations of amyloid cores of prion strains. Some tyrosine residues (shown in blue) are experiencing different local environment and orientation, reflecting presumably differences on the packing of the prion core between the two strains.

observed wavelength dependence of the LD spectrum (39). For both prion strains the simulation of the absorption and LD spectra (Fig. 4 *C* and *D*) is consistent with one dominating blue-shifted fraction of tyrosines oriented near 30° (for L_b) in a non-polar environment (presumably in the interior of the hydrophobic fiber core). The remaining tyrosines may be blue-shifted or red-shifted, depending on whether they are hydrogen bond donors or hydrogen bond acceptors (38). We think that tyrosines located in "intermediate" regions of the amyloid core (25) are able to adopt different orientations compared with the residues that are buried in the interior of the rigid regions (Fig. 5). In proteins, aromatic rings in exposed regions are considered to have less constraint in their motion than buried rings (40). According to solid-state NMR spectroscopy studies of Sup35NM fibers, tyrosine residues outside the amyloid rigid core are in beta-strand conformation but in a different environment compared with the core residues (24). Additionally, the aromatic interactions outside the amyloid core are considered to drive the aggregation of different Sup35NM monomers (41). If aromatic rings outside the amyloid core are freely rotating they will not contribute to the LD signal. However, if they are somehow oriented but their environment is different this will cause a shift in the transition energies, resulting in a shift of the LD band compared to the absorption band and accordingly in a variation of the LD/A_{iso} with wavelength. This indicates that in Sup35 prion strains there is some heterogeneity in orientation and environment of the tyrosine residues, which will contribute to differentiate the strains. The different biological performance of the strains can thus originate from variations in packing of beta-sheet building blocks, which is to say that the building blocks find different ways of sticking together depending on the environmental conditions.

The present approach provides insight about organization and assembly of amyloid-prone protein aggregates. LD is capable of detecting variations in the tyrosine chromophore location, solvent-exposed vs. buried tyrosines, reflecting on the packing of the prion core. We are only beginning to understand how aromatic residues are spatially arranged in amyloid fibers. We cannot determine yet which tyrosine residues are differently oriented in the two strains, but the replacement of a single tyrosine by phenylalanine will allow obtaining angular data in a corresponding way for a series of selected residues (site-selected LD). LD promises thus to have broad application to structural investigations of amyloids.

Materials and Methods

Sample Preparation. Recombinant prion domain of the yeast prion protein Sup35NM was expressed and purified as described elsewhere (42). The protein concentration was determined by UV/visible using a theoretical extinction coefficient of 25,600 $M^{-1}{\cdot}cm^{-1}$. Purified protein in 8 M urea was desalted by addition of five volumes of methanol, storage at −80 °C, and centrifugation at 4 °C for 15 min at 15,000 × *g*. Protein was recovered as a white pellet. Yeast prion fiber seeds were prepared from an in vivo prion template as described elsewhere (25). Strain-specific prion fiber samples were prepared by resuspending methanol-precipitated NM protein in 5% (monomer concentration) solutions of strain-specific seeds and incubation at either 4 °C (strong prion fibers) or 37 °C (weak prion fibers) in 10 mM Tris·HCl (pH 7.4) and 150 mM sodium chloride. The prion fiber samples (5 mg/mL) were diluted to a concentration of 0.5 mg/mL either with ultrapure water containing probes (ThT) or with 50% wt/wt sucrose aqueous solution for LD flow experiments. The polymer matrix was prepared with 10 wt/wt% of PVA (with molecular weight *ca*. 80,000) (Elvanol 71-30; DuPont) in ultrapure water, heated to about 90 °C with vigorous stirring for 2 h. PVA solution was allowed to cool down to room temperature and, after careful mixing with prion fiber sample, the solution was spread on a glass surface as a thin layer and left to dry at room temperature for at least 2 d. The final concentration of fibers was 0.5 mg/mL.

LD and Absorbance Measurements. LD and absorbance spectra were recorded on a Chirascan instrument (Applied Photophysics Ltd.) in two different media: (*i*) in aqueous solution subjected to shear flow and (*ii*) in a humid gel of PVA subjected to mechanical stretch. To avoid artifacts owing to different monochromator dispersion and different scattering angles, LD and absorbance spectra were measured on the same instrument. The spectra were corrected by subtracting a scattering profile represented by a Rayleigh scattering model (*Supporting Information*).

Flow solution experiments were performed with a Couette cell that consists of two concentric quartz (fused silica, Suprasil; Hellma) cylinders, one static (the inner one) and one rotating (the outer one) (Fig. 1). Light passes through both cylinders along the radius of the cylinders, thereby passing two times through the sample, which is contained in the annular gap in between the cylinders (cell path length is 1 mm and the sample volume is about 2.0 mL). To improve the measuring sensitivity in the far UV region sucrose was added as a refractive index matching agent. This is found to eliminate or strongly reduce the light scattering but also to improve the orientation as a result of increased solvent viscosity and thereby attenuated rotary diffusion (increased ratio G/D_{rot}).

Stretched PVA hydrogel experiments were performed with the help of a stretching device (Fig. 1). A fragment, *ca*. 2 × 2 cm, was cut from the dry film and mounted in a stretching device, which was then inserted into a humidity chamber and allowed to equilibrate with a pure water solution at the bottom of the chamber, giving 100% relative humidity. In practice this was found to yield a PVA hydrogel containing about 50% water. The humid film was stretched at room temperature to various degrees of stretch, defined as the length ratio l/l_0, l being the total length of the stretched film, l_0 the length in unstretched state. We shall denote l/l_0 as R_S', which is connected to the "stretch ratio" R_S in the Kratky model according to the relation $R_S = (R_S')^{3/2}$ (30).

ACKNOWLEDGMENTS. This work was supported by King Abdullah University of Science and Technology Grant KUK-11-008-23, European Research Council Grant EC-2008 AdG 227700-SUMO, Swedish Research Council Linnaeus Grant SUPRA 349-2007-8680, Howard Hughes Medical Institute (HHMI), and National Institutes of Health Grant GM025874 (to S.L.). K.K.F. was an HHMI Fellow of the Life Science Research Foundation.

1. Knowles TPJ, Vendruscolo M, Dobson CM (2014) The amyloid state and its association with protein misfolding diseases. *Nat Rev Mol Cell Biol* 15:384–396.

2. Blanco LP, Evans ML, Smith DR, Badtke MP, Chapman MR (2012) Diversity, biogenesis and function of microbial amyloids. *Trends Microbiol* 20(2):66–73.

3. Heinrich SU, Lindquist S (2011) Protein-only mechanism induces self-perpetuating changes in the activity of neuronal Aplysia cytoplasmic polyadenylation element binding protein (CPEB). *Proc Natl Acad Sci USA* 108(7):2999–3004.
4. Majumdar A, et al. (2012) Critical role of amyloid-like oligomers of Drosophila Orb2 in the persistence of memory. *Cell* 148(3):515–529.
5. Wickner RB (1994) [URE3] as an altered URE2 protein: Evidence for a prion analog in Saccharomyces cerevisiae. *Science* 264(5158):566–569.
6. Paushkin SV, Kushnirov VV, Smirnov VN, Ter-Avanesyan MD (1997) In vitro propagation of the prion-like state of yeast Sup35 protein. *Science* 277(5324):381–383.
7. Du Z, Park K-W, Yu H, Fan Q, Li L (2008) Newly identified prion linked to the chromatin-remodeling factor Swi1 in Saccharomyces cerevisiae. *Nat Genet* 40(4):460–465.
8. Halfmann R, et al. (2012) Prions are a common mechanism for phenotypic inheritance in wild yeasts. *Nature* 482(7385):363–368.
9. True HL, Lindquist SL (2000) A yeast prion provides a mechanism for genetic variation and phenotypic diversity. *Nature* 407(6803):477–483.
10. Tanaka M, Chien P, Naber N, Cooke R, Weissman JS (2004) Conformational variations in an infectious protein determine prion strain differences. *Nature* 428(6980): 323–328.
11. King C-Y, Diaz-Avalos R (2004) Protein-only transmission of three yeast prion strains. *Nature* 428(6980):319–323.
12. Sparrer HE, Santoso A, Szoka FC, Jr, Weissman JS (2000) Evidence for the prion hypothesis: Induction of the yeast [PSI+] factor by in vitro- converted Sup35 protein. *Science* 289(5479):595–599.
13. Chien P, Weissman JS, DePace AH (2004) Emerging principles of conformation-based prion inheritance. *Annu Rev Biochem* 73:617–656.
14. Prusiner SB, Scott MR, DeArmond SJ, Cohen FE (1998) Prion protein biology. *Cell* 93(3): 337–348.
15. Guo JL, et al. (2013) Distinct α-synuclein strains differentially promote tau inclusions in neurons. *Cell* 154(1):103–117.
16. Kodali R, Williams AD, Chemuru S, Wetzel R (2010) Abeta(1-40) forms five distinct amyloid structures whose beta-sheet contents and fibril stabilities are correlated. *J Mol Biol* 401(3):503–517.
17. Nekooki-Machida Y, et al. (2009) Distinct conformations of in vitro and in vivo amyloids of huntingtin-exon1 show different cytotoxicity. *Proc Natl Acad Sci USA* 106(24):9679–9684.
18. Petkova AT, et al. (2005) Self-propagating, molecular-level polymorphism in Alzheimer's beta-amyloid fibrils. *Science* 307(5707):262–265.
19. Jucker M, Walker LC (2013) Self-propagation of pathogenic protein aggregates in neurodegenerative diseases. *Nature* 501(7465):45–51.
20. Polymenidou M, Cleveland DW (2012) Prion-like spread of protein aggregates in neurodegeneration. *J Exp Med* 209(5):889–893.
21. Watts JC, et al. (2013) Transmission of multiple system atrophy prions to transgenic mice. *Proc Natl Acad Sci USA* 110(48):19555–19560.
22. Krishnan R, Lindquist SL (2005) Structural insights into a yeast prion illuminate nucleation and strain diversity. *Nature* 435(7043):765–772.
23. Toyama BH, Kelly MJS, Gross JD, Weissman JS (2007) The structural basis of yeast prion strain variants. *Nature* 449(7159):233–237.
24. Luckgei N, et al. (2013) The conformation of the prion domain of Sup35cp in isolation and in the full-length protein. *Angew Chemie Int* 52(48):12741–12744.
25. Frederick KK, et al. (2014) Distinct prion strains are defined by amyloid core structure and chaperone binding site dynamics. *Chem Biol* 21(2):295–305.
26. Adachi R, et al. (2007) Flow-induced alignment of amyloid protofilaments revealed by linear dichroism. *J Biol Chem* 282(12):8978–8983.
27. Andersen CB, et al. (2010) Glucagon fibril polymorphism reflects differences in protofilament backbone structure. *J Mol Biol* 397(4):932–946.
28. Hamley IW, et al. (2010) Alignment of a model amyloid Peptide fragment in bulk and at a solid surface. *J Phys Chem B* 114(24):8244–8254.
29. Tanizaki Y (1959) Dichroizm of dyes in the stretched PVA sheet. II. The relation between the optical density ratio and the stretch ratio, and an attempt to analyze relative directions of absorption bands. *Bull Chem Soc Jpn* 32:75–80.
30. Nordén B (1980) Simple formulas for dichroism analysis. Orientation of solutes in stretched polymer matrices. *J Chem Phys* 72:5032–5038.
31. Kitts CC, Vanden Bout DA (2009) Near-field scanning optical microscopy measurements of fluorescent molecular probes binding to insulin amyloid fibrils. *J Phys Chem B* 113(35):12090–12095.
32. Ardhammar M, Lincoln P, Nordén B (2002) Invisible liposomes: Refractive index matching with sucrose enables flow dichroism assessment of peptide orientation in lipid vesicle membrane. *Proc Natl Acad Sci USA* 99(24):15313–15317.
33. Uptain SM, Sawicki GJ, Caughey B, Lindquist S (2001) Strains of [PSI(+)] are distinguished by their efficiencies of prion-mediated conformational conversion. *EMBO J* 20(22):6236–6245.
34. Castro CE, Dong J, Boyce MC, Lindquist S, Lang MJ (2011) Physical properties of polymorphic yeast prion amyloid fibers. *Biophys J* 101(2):439–448.
35. Gazit E (2002) A possible role for pi-stacking in the self-assembly of amyloid fibrils. *FASEB J* 16(1):77–83.
36. Jack E, Newsome M, Stockley PG, Radford SE, Middleton DA (2006) The organization of aromatic side groups in an amyloid fibril probed by solid-state 2H and 19F NMR spectroscopy. *J Am Chem Soc* 128(25):8098–8099.
37. McGaughey GB, Gagné M, Rappé AK (1998) π-Stacking interactions. Alive and well in proteins. *J Biol Chem* 273(25):15458–15463.
38. Fornander LH, Feng B, Beke-Somfai T, Norden B (2014) The UV transition moments of tyrosine. *J Phys Chem B* 118(31):9247–9257.
39. Eriksson M, Norden B, Jernstroem B, Graeslund A (1988) Binding geometries of benzo [a]pyrenediol epoxide isomers covalently bound to DNA. Orientational distribution. *Biochemistry* 27(4):1213–1221.
40. Gall CM, Cross TA, DiVerdi JA, Opella SJ (1982) Protein dynamics by solid-state NMR: Aromatic rings of the coat protein in fd bacteriophage. *Proc Natl Acad Sci USA* 79(1): 101–105.
41. Ohhashi Y, Ito K, Toyama BH, Weissman JS, Tanaka M (2010) Differences in prion strain conformations result from non-native interactions in a nucleus. *Nat Chem Biol* 6:225–230.
42. Serio TR, Cashikar AG, Moslehi JJ, Kowal AS, Lindquist SL (1999) Yeast prion [psi +] and its determinant, Sup35p. *Methods Enzymol* 309:649–673.